Mon. Not. R. Astron. Soc. **270**, 390–400 (1994)

Alignment and morphology of elliptical galaxies: the influence of the cluster tidal field

L. Ciotti[1,2] and S.N. Dutta[2]

[1]*Osservatorio Astronomico di Bologna, via Zamboni 33, Bologna 40126, Italy*
[2]*Princeton University Observatory, Peyton Hall, Princeton 08544, NJ, USA*

Accepted 1994 April 28. Received 1994 January 31; in original form 1993 September 21

ABSTRACT

We investigate two possible effects of the tidal field induced by a spherical cluster on its elliptical galaxy members: the modification of the ellipticity of a spherical galaxy and the isophotal alignment in the cluster radial direction of a misaligned prolate galaxy. Numerical N-body simulations have been performed for radial and circular galactic orbits. The properties of the stars' zero-velocity surfaces in the perturbed galaxy are explored briefly, and the adiabaticity of the galaxy to the external field is discussed. For a choice of parameters characteristic of rich clusters, we find that the induced ellipticity on a spherical galaxy is below or close to the detectability level. But we find that the tidal torque can result in significant isophotal alignment of the galaxy's major axis with the cluster radial direction if the galaxy is outside the cluster core radius. The time required for the alignment is very short compared with the Hubble time. A significant increase in the ellipticity of the outer isophotes of the prolate model is also found, but with no observable isophotal twisting. Our main prediction is an alignment segregation of the elliptical galaxy population according to whether their orbits lie mostly outside or inside the cluster core radius. These results also suggest that galactic alignment in rich clusters is not incompatible with a bottom-up galaxy formation scenario.

Key words: galaxies: clustering – galaxies: elliptical and lenticular, cD – galaxies: interactions – galaxies: kinematics and dynamics – galaxies: photometry – galaxies: structure.

1 INTRODUCTION

The morphology of elliptical galaxies (Es) is used to a considerable extent to acquire information about their structure and evolution. This is justified, to the first approximation, by the fact that their internal two-body relaxation time is longer than the Hubble time, so the shape and the internal dynamics of Es probably reflect the conditions immediately after the end of their formation processes.

The problem with this naïve scenario is that Es in clusters are not isolated objects, and are subject to the effects of their environment, many of which act on time-scales shorter than the Hubble time. Consequently it is of utmost importance to be able to isolate the effects of the environment when attempting to decipher the initial conditions from the present. Also these effects are of intrinsic interest as a source of information on the environment. In some cases the past interactions are signalled by the presence of shells, counter-rotating cores, polar rings, dust lanes, etc., which are taken to be evidence for merging events in the history of the galaxy. In other cases we know that strong environmental effects have to be present, for example in interacting galaxies and galaxies in groups.

Another group of interactions comprises the hyperbolic encounters between galaxies in rich (well relaxed) clusters, and the effect of the mean cluster tidal field (CTF), both of which are poorly understood. In particular the CTF acts continuously, and affects more or less all the galaxies in the cluster. So we expect that, even if the CTF is not as strong as other interactions, it is possible to detect its effects through systematic (albeit small) differences between cluster and field galaxies. Related to this is the cosmological problem raised by a possible large-scale alignment of the major axes of Es along some preferred direction in the parent cluster: alignment is viewed as a consequence of top-down galaxy formation scenarios because it is usually believed that, in a bottom-up cluster formation, Es would be characterized by random orientation (see Djorgovski 1987 for a review).

There have been a large number of photometric studies to search for global correlations of Es' properties, such as ellipticities or the position angles of their major axes with their positions in their parent cluster. As far as any systematic differences between cluster and field Es are concerned, the results are generally in the negative. Thompson (1976) did not find any difference between the ellipticity distributions of Coma Es and field ellipticals; Fasano & Bonoli (1989) studied the occurrence of isophotal twisting in isolated galaxies, and found essentially the same fraction of isophotal twist as in cluster galaxies. Lambas, Maddox & Loveday (1992), in a

© Royal Astronomical Society • Provided by the NASA Astrophysics Data System

homogeneous and very big sample, found that 'the projected distributions of axial ratios of high and low local density environment ellipticals are remarkably similar'. So they 'see no evidence in the data that the environment has significantly affected the shapes of Es'. Porter, Schneider & Hoessel (1991) studied the brightest cluster ellipticals (BCE) in elongated Abell clusters and did not find a correlation between BCE shape and environment or cluster properties.

Moving to the alignment problem, there are no firmly established results. Hawley & Peebles (1975) reported 'a possible indication that the galaxies are preferentially aligned along the radius vector to the center of the cluster' for the Coma cluster, a result confirmed by Thompson (1976), and suggested the CTF as a possible cause in aligning the galaxies. MacGillivray & Dodd (1979a,b) found that 'there are systematic alignment tendencies for galaxies which are members of the loose cluster centred on the galaxy NGC 439 in the sense that the galaxies are preferentially aligned either parallel with the radius vector from NGC 439 or perpendicular to it'. For another rich and symmetrical cluster they found a preferential alignment of Es' major diameters in the cluster radial direction. Adams, Strom & Strom (1980) found, in 7 very elongated clusters, a general trend for Es to be aligned with the cluster major axis, and for the cluster A2197 they confirmed the results of Thompson (1976). They also found a small but significant number of Es with their major axes perpendicular to the cluster major axis. Fong, Stevenson & Shanks (1990) found a moderately significant radial alignment of Es, together with a less significant tendency for Es to be oriented perpendicular to this direction. The best evidence for alignment is for the BCE. Trevese, Cirimele & Flin (1992) found 'a strong alignment of the brightest galaxy major axis with the long axis of the parent cluster' but 'no significant alignment for galaxies fainter than the first two'. In this particular case the alignment is believed to be due to accretion. Rhee & Roos (1990) performed N-body simulations in which they found the BCE alignment to be effected during the cluster collapse.

This paper is devoted to the study of the influence of the CTF of a rich cluster in determining the properties of its member Es. The first of the two effects studied is the change of the ellipticity of the isophotal contours of the galaxies with increasing distance from their centres, and the second is the isophotal alignment of a prolate galaxy in the cluster radial direction. The cluster is treated as an externally imposed homogeneous, spherically symmetric stationary field and we evolve, using an N-body code, spherical and prolate galaxies for many galactic dynamical times in circular and radial orbits about the cluster centre. In Section 2 we describe in detail the properties of the cluster and the spatial and projected properties of the galaxy models for the initial conditions we use for the simulations. In Section 3 we derive analytically the expressions for the CTF and we study the adiabaticity of the response of spherical galaxies in radial orbits and of prolate galaxies held stationary to the tidal field. Galaxies that are in orbits that sample the most interesting parts of the CTF, according to this analytical study, are evolved numerically. In Section 4 the determination of the numerical initial conditions is briefly explained, and in Section 5 we show the results of the numerical simulations. In Section 6 we present our conclusions.

2 THE MODELS

2.1 Cluster characteristics

For the smoothed, zeroth-order density distribution that describes the cluster used in our simulations, we assume the distribution given by King (1972) to fit the Coma cluster:

$$\rho_c(r) = \frac{\rho_{c0}}{(1 + r^2/r_c^2)^{3/2}}, \tag{1}$$

where $r = |\boldsymbol{r}|$ is the distance from the cluster centre, $r_c = 171\,\mathrm{kpc}$ is the 'core' radius, and the distribution is truncated at some r_t. We derive the central density from the well-known formula $\rho_{c0} = 9\sigma_c^2/4\pi G r_c^2 \simeq 6.4 \times 10^{-3}\,\mathrm{M_\odot\,pc^{-3}}$ (e.g. Binney & Tremaine 1987, hereafter BT87, p. 228), assuming the cluster central velocity dispersion $\sigma_c = 1.061 \times 10^3\,\mathrm{km\,s^{-1}}$. The assumption of a spherical cluster is a very idealized one, but is justified by the fact that we want to model galaxies on which a stationary cluster field has acted for a long time, so we are considering relaxed clusters, which are characterized by spherical symmetry. The same cluster density distribution (although with different parameters) is used for example by Valluri (1993) to investigate (without taking into account the self-gravity of the galaxy) the response of a disc galaxy to the CTF.

2.2 Spherical galaxy characteristics

In order to study the effect of the CTF in deforming the shapes of Es, we assume as initial conditions for the N-body simulations a Plummer galaxy model, described by the density-potential pair:

$$\rho(\xi) = \frac{3}{4\pi}\frac{M_g}{r_P^3}\frac{1}{(1+\tilde{\xi}^2)^{5/2}}, \tag{2}$$

$$\phi_P(\xi) = -\frac{GM_g}{r_P}\frac{1}{\sqrt{1+\tilde{\xi}^2}}, \tag{3}$$

where M_g is the total mass of the galaxy, r_P is the core radius of the Plummer sphere, and $\tilde{\xi} = |\xi|/r_P$ is the distance from the centre of mass of the galaxy expressed in units of r_P. To quantify the galactic scale length on which the deformation can be observed, we use the projected density profile of the unperturbed galaxy:

$$\Sigma(R) = \frac{M_g}{\pi r_P^2(1+\tilde{R}^2)^2}, \tag{4}$$

where $\tilde{R} = R/r_P$ is the normalized projected radius, and from that, assuming a constant mass-to-light ratio, we derive

$$\mu(R) - \mu(0) = 5\log(1+\tilde{R}^2), \tag{5}$$

where $\mu(R) \equiv -2.5\log\Sigma(R) + \text{constant}$. For example $R = 10r_P$ corresponds to a 10-mag fading of the projected surface brightness. Integrating (4) on a circular aperture one obtains the expression for the cumulative projected mass inside R, and the effective radius $R_e = r_P$. In order to determine a galaxy model we have to assign realistic values for the parameters in (2). We choose $M_g = 10^{12}\,\mathrm{M_\odot}$ and $r_P = 5.0\,\mathrm{kpc}$, so the model represents a giant elliptical. The order of magnitude estimate for the half-mass radius dynamical time is $t_{dyn} \equiv 1/\sqrt{G\bar{\rho}} \simeq 2.3 \times 10^7\,\mathrm{yr}$, where $\bar{\rho} = 1.5M_g/4\pi r_h^3$ is the mean density of the galaxy inside the half-mass radius, $r_h = r_P/\sqrt{2^{2/3}-1}$.

© Royal Astronomical Society • Provided by the NASA Astrophysics Data System

2.3 Prolate galaxy characteristics

For the analysis of the alignment of a non-spherical galaxy due to the torque induced by the CTF, we start by assuming as initial conditions for the N-body simulations a density distribution reproducing a prolate galaxy. Its density distribution is stratified in homeoids labelled by $m^2 = x^2/r_P^2 + y^2/r_P^2 + z^2/(r_P^2\lambda)$ and $\lambda \geq 1$:

$$\rho(m) = \frac{3M_g}{16\pi\sqrt{\lambda}r_P^3} \times \begin{cases} 1, & \text{if } m \leq 1, \\ m^{-4}, & \text{otherwise.} \end{cases} \tag{6}$$

We use (6) instead of the more natural generalization of (2) because it is easier to obtain the potential needed to compute the internal velocity dispersion (see Section 4). We choose the total mass M_g and the 'core' radius r_P equal to the corresponding values used for the spherical model, and $\lambda = 2$. The half-mass radius dynamical time is $t_{dyn} \simeq 3.3 \times 10^7$ yr, the half-mass homeoid being labelled by $m = 3/2$.

As in the previous case, to obtain information on the galaxy modifications we project (6) along the y axis. The resulting surface density distribution is

$$\Sigma(l) = \frac{3M_g}{16\pi\sqrt{\lambda}r_P^2} \begin{cases} [l\sqrt{1-l^2}(2l^2-1) + \arcsin l]/l^3, \\ \pi/2l^3, \end{cases} \tag{7}$$

where $l^2 = x^2/r_P^2 + z^2/(r_P^2\lambda)$ and the first expression holds for $l \leq 1$. Integrating over ellipses of constant l one can easily determine the effective isophote l_e, i.e. the isophote that contains half of the total mass. After a little algebra we have that $l_e = 3\pi/8$, i.e. the short semi-axis of the effective isophote is $\simeq r_P$. This is consistent with the longer half-mass dynamical time with respect to the spherical model. The radial behaviour of the surface brightness profile, for $l \geq 1$, is given by

$$\mu(l) - \mu(0) = 2.5\log\left(\frac{16l^3}{3\pi}\right) \simeq 0.58 + 7.5\log l. \tag{8}$$

3 ANALYTICAL ESTIMATE OF A GALAXY RESPONSE

In this section we derive and study the expression for the CTF and its fundamental properties as a function of the distance from the cluster centre. Following that we briefly describe the effects of the CTF on a spherical galaxy in radial and circular orbits, using the zero-velocity surfaces of its stars. Finally we discuss the response of a galaxy in a radial orbit and of a prolate galaxy misaligned with the cluster radial direction to the variation of the CTF, using a quantitative estimate of the galaxy adiabaticity.

3.1 Cluster tidal field

Let $C = (O; \boldsymbol{e}_1, \boldsymbol{e}_2, \boldsymbol{e}_3)$ be an inertial reference system centred on the cluster, with $\boldsymbol{r}$ as a generic position vector, and $C' = (O'; \boldsymbol{f}_1, \boldsymbol{f}_2, \boldsymbol{f}_3)$, with $\boldsymbol{\xi}$ as the generic position vector, be a second reference system centred on $\boldsymbol{r}_g = \int \rho(\boldsymbol{r}; t)\boldsymbol{r}\mathrm{d}^3\boldsymbol{r}/M_g$, the centre of mass of the galaxy. The system C' is allowed to rotate with an angular velocity $\boldsymbol{\Omega}$ (viewed from the frame C'). This is the natural system to study the response of the galaxy to the CTF. Using the usual rules of transformation (see e.g. Arnold 1978), the positions, velocities and accelerations in the two frames are related as follows:

$$\begin{aligned} \boldsymbol{r} &= \boldsymbol{r}_g + \mathcal{O}\boldsymbol{\xi}, \\ \dot{\boldsymbol{r}} &= \boldsymbol{v}_g + \mathcal{O}(\boldsymbol{\Omega}\wedge\boldsymbol{\xi} + \dot{\boldsymbol{\xi}}), \\ \ddot{\boldsymbol{\xi}} &= \mathcal{O}^{\mathrm{T}}(\ddot{\boldsymbol{r}}_{self} + \ddot{\boldsymbol{r}}_{ext} - \boldsymbol{a}_g) \\ &\quad - 2\boldsymbol{\Omega}\wedge\dot{\boldsymbol{\xi}} - \dot{\boldsymbol{\Omega}}\wedge\boldsymbol{\xi} - \boldsymbol{\Omega}\wedge(\boldsymbol{\Omega}\wedge\boldsymbol{\xi}), \end{aligned} \tag{9}$$

where the last three terms on the right hand side are the Coriolis Force, Euler's Force and the Centrifugal Force, respectively, and $\mathcal{O}$ is the orthogonal transformation matrix (generally time-dependent) between C and C'.

The acceleration terms in parentheses are the fields acting on each star due to the parent galaxy, that due to the cluster and the acceleration of the galaxy centre of mass, respectively. The CTF is given by the linearization of $\ddot{\boldsymbol{r}}_{ext} - \boldsymbol{a}_g$, where, using Jeans' equations, $M_g\boldsymbol{a}_g = \int \rho(\boldsymbol{r}; t)(\ddot{\boldsymbol{r}}_{self} + \ddot{\boldsymbol{r}}_{ext})\mathrm{d}^3\boldsymbol{r} = \int \rho(\boldsymbol{r}; t)\ddot{\boldsymbol{r}}_{ext}\mathrm{d}^3\boldsymbol{r}$. Linearizing the cluster field around $\boldsymbol{r}_g$ and defining $r_g = |\boldsymbol{r}_g|$, one obtains

$$\begin{aligned} \frac{M_c(r)}{r^3}r_i = \frac{M_c(r_g)}{r_g^3}r_{gi} + \\ \left[\delta_{ij}\frac{M_c(r_g)}{r_g^3} + \frac{r_{gi}r_{gj}}{r_g}\frac{\partial}{\partial r_g}\frac{M_c(r_g)}{r_g^3}\right](r_j - r_{gj}), \end{aligned} \tag{10}$$

where the expansion is truncated to the order $O(|\boldsymbol{r} - \boldsymbol{r}_g|^2)$ and δ_{ij} is the Kronecker symbol. Fixing the orientation of C' in such a way that $\boldsymbol{r}_g$ is parallel to $\boldsymbol{f}_1$, the linearized external field in (9) can be written as

$$T_i = \mathcal{T}_{ij}\xi_j + \mathcal{R}_i, \tag{11}$$

where $\mathcal{R}_i$ is the ith-component of the non-inertial forces and the expression of the (symmetric) CTF tensor is

$$\mathcal{T}(r_g) = -\frac{4\pi G\bar{\rho}_c}{3}\begin{pmatrix} 3q-2 & 0 & 0 \\ 0 & 1 & 0 \\ 0 & 0 & 1 \end{pmatrix}, \tag{12}$$

where $\bar{\rho}_c = 3M_c(r_g)/(4\pi r_g^3)$ and $0 \leq q(r_g) = \rho_c(r_g)/\bar{\rho}_c \leq 1$ for any non-increasing density distribution. One can check equation (12) by showing that the trace of the tidal tensor equals $-4\pi G\rho_c$ as required by the Poisson equation. From (1) one obtains

$$q(\tilde{r}_g) = \frac{\tilde{r}_g^3}{3(1+\tilde{r}_g^2)^{3/2}[\operatorname{arsinh}(\tilde{r}_g) - \tilde{r}_g/\sqrt{1+\tilde{r}_g^2}\,]}, \tag{13}$$

where $\tilde{r}_g = r_g/r_c$. The solid line in Fig. 1 shows the variation of q with the distance from the cluster centre.

We can investigate the geometry of the CTF by looking at its potential, i.e. $\mathcal{T}_{ij}\xi_j = -\partial\tau/\partial\xi_i$, with

$$\tilde{\tau} = (3q-2)\tilde{\xi}_1^2 + \tilde{\xi}_2^2 + \tilde{\xi}_3^2, \tag{14}$$

where $\tilde{\tau}$ is the potential, τ, normalized to $2\pi G\bar{\rho}_c r_P^2/3$. The general property of $\tilde{\tau}$ = constant surfaces is their axisymmetry about the $\tilde{\xi}_1$ axis (i.e. the direction to the centre of the cluster) and symmetry with respect to reflection about the $\tilde{\xi}_2$–$\tilde{\xi}_3$ plane. We distinguish two different regions in the cluster.

For $2/3 < q \leq 1$, i.e. for $1.027 > \tilde{r}_g \geq 0$ (Fig. 1, region to the left of the vertical dashed line), the isopotential surfaces are prolate ellipsoids with their major axes in the cluster radial direction. The tidal potential increases with r_g with the equipotential surfaces forming a family of similar ellipsoids, i.e. inside the cluster core the CTF is everywhere compressive. For $q = 1$ (in the cluster centre or in the case of an homogeneous

© Royal Astronomical Society • Provided by the NASA Astrophysics Data System

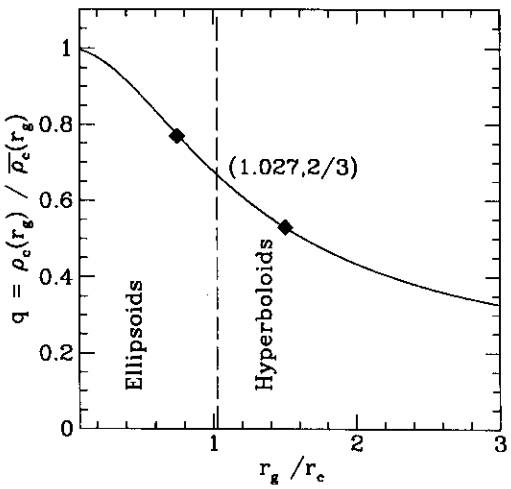

Figure 1. The solid line is the radial trend of the function $q = q(r_g/r_c)$. The vertical dashed line separates the two regions of the cluster that correspond to qualitatively different shapes of the tidal potential. The two black diamonds are the positions of the models calculated in circular orbits and the apocentres of radial orbits.

spherical density distribution) the CTF is radially compressive about the galaxy centre.

For $q = 2/3$ (Fig. 1, vertical dashed line) the isopotential surfaces are cylinders with their axes along $\tilde{\xi}_1$, and in this case the CTF is radially compressive around this axis.

For $0 \leq q < 2/3$ (Fig. 1, region to the right of the vertical dashed line) the coefficient of $\tilde{\xi}_1$ is negative. The quadratic form (14) is no longer positive definite and the value of the potential can be positive or negative, without lower or upper limits. The isopotential surfaces are two-sheet and one-sheet similar hyperboloids of revolution around the cluster radial direction, for negative and positive $\tilde{\tau}$ values, respectively. The two families are separated by the $\tilde{\tau} = 0$ asymptotic cone, the angle of which gets smaller as q increases (i.e. r_g decreases). In this last radial region the CTF is expansive along $\tilde{\xi}_1$ and radially compressive perpendicular to this axis.

So the cluster core radius ($\tilde{r}_g = 1$) marks the transition region between two qualitatively different CTFs, and we expect this distance to be a point of bifurcation of the Es' properties. We move now to obtain some hint of the response of a spherical galaxy in radial and circular orbits in the cluster. We do this in an approximate way by adding the appropriate tidal potential to the unperturbed galaxy potential. This is clearly not a self-consistent way of analysing the problem, but in this case is not too wrong: the CTF *increases* linearly with the distance from the galaxy centre while its self-gravity in the external regions *decreases* roughly as the square of this distance. So the effects of the CTF are more important in the external parts of the galaxy. Moreover we assume that the local galaxy density is produced approximately by stars near their zero-velocity surfaces. The stars spend the most of their orbital time near these surfaces, justifying their use.

3.2 Radial galaxy orbit

If we consider a galaxy in a perfectly radial orbit, all the non-inertial terms due to the rotation vanish, i.e. $\mathscr{R}_i = 0$ $(i = 1, 2, 3)$ in (11), and the system C' is determined by requiring that the vector $\boldsymbol{f}_1$ lie in the direction of $\boldsymbol{r}_g$. For our models the axial ratios of the zero-velocity surfaces near the galaxy's centre are very near to one, i.e. the effect of the CTF in the central galaxy regions is negligible. In Fig. 2 the behaviour of sections of the isopotential surfaces is shown for two different positions of the galaxy in the cluster. It is evident that in both the positions the surfaces remain approximately spherical inside $5R_e$, and only outside do they become prolate in the cluster radial direction.

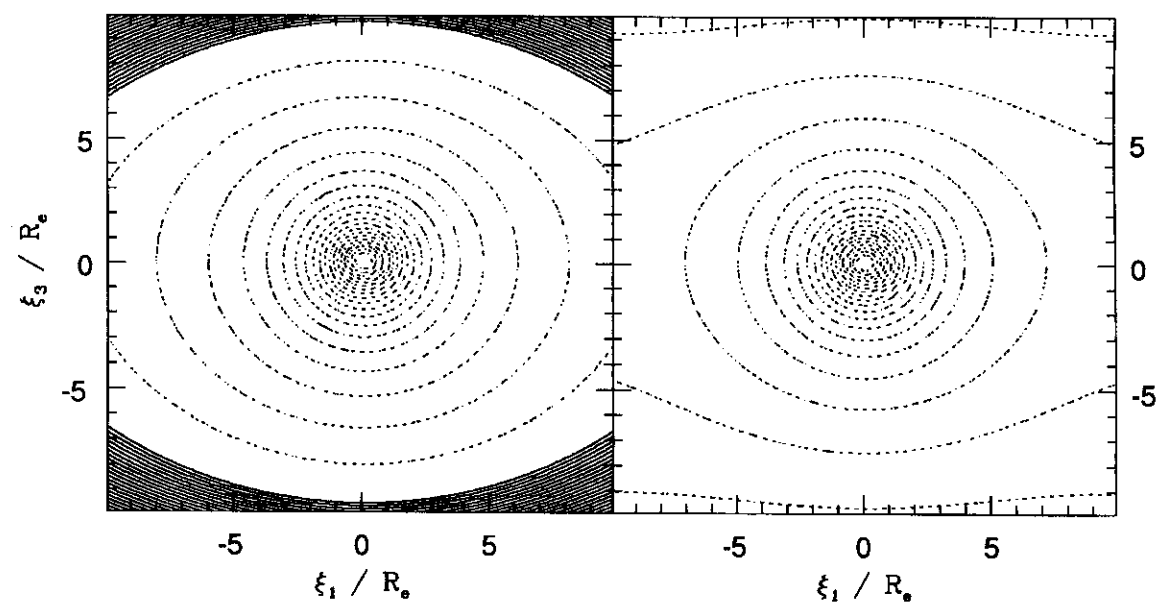

Figure 2. Sections of the stars' zero-velocity surfaces in the $\tilde{\xi}_1 - \tilde{\xi}_3$ plane, in the model galaxy (2) in a radial orbit. In the left panel the sections for $\tilde{r}_g = 0.75$ ($q \simeq 0.77$) are shown, and those for $\tilde{r}_g = 1.5$ ($q \simeq 0.53$) are shown in the right panel. Dashed and solid lines refer to negative and positive potential (galaxy + cluster) values respectively.

© Royal Astronomical Society • Provided by the NASA Astrophysics Data System

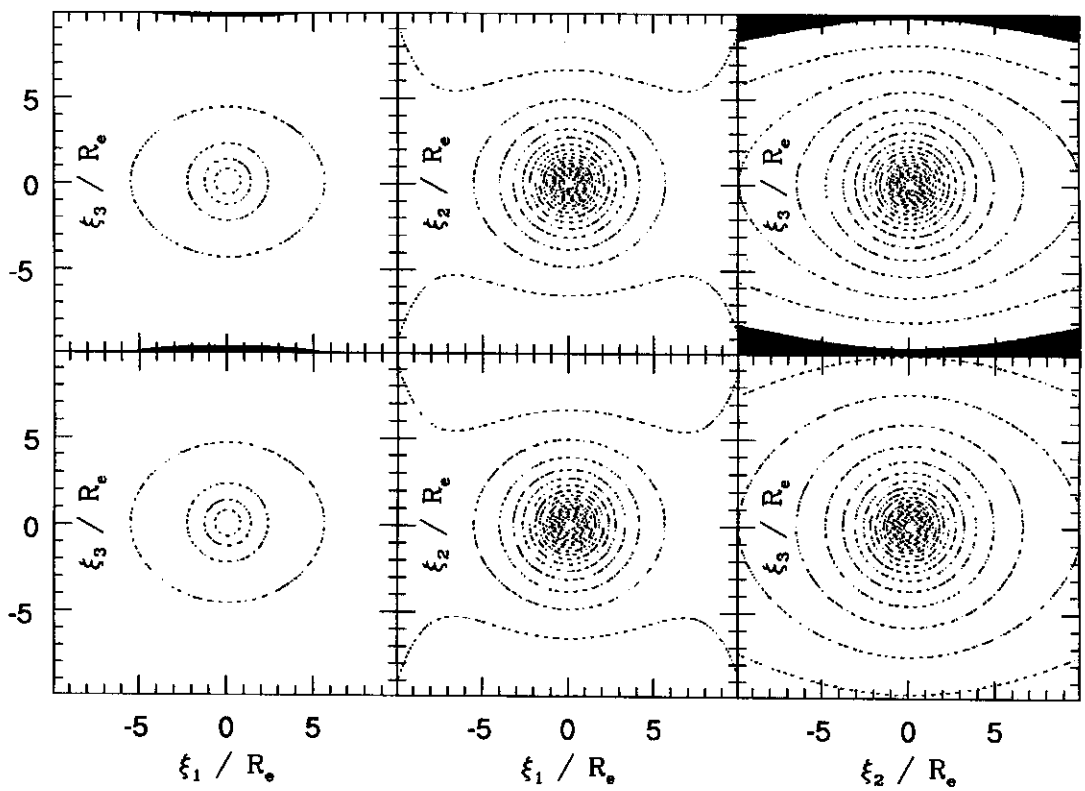

Figure 3. Sections of the stars' zero-velocity surfaces for the model galaxy (2) in circular orbits. From left to right the sections are respectively in the planes $\tilde{\xi}_2 = 0$, $\tilde{\xi}_3 = 0$, and $\tilde{\xi}_1 = 0$. In the three upper panels the galaxy orbit is inside the cluster core radius at $\tilde{r}_g = 0.75$, and in the three lower ones the galaxy orbit is at $\tilde{r}_g = 1.5$. Dashed and solid lines refer to negative and positive potential (galaxy + cluster) values respectively.

3.3 Circular galaxy orbit

In this case the galaxy is in a circular orbit of radius r_g around the cluster centre. This assumption implies that in the expression for $\mathscr{R}_i$ the Euler force vanishes and the Jacobi integral is conserved by each star (e.g. BT87, p. 135). The coordinate system C' is determined by requiring that the vector $\boldsymbol{f}_1$ lie in the direction of $\boldsymbol{r}_g$, and that $\boldsymbol{f}_3$ be parallel to $\boldsymbol{\Omega}$. The zero-velocity surfaces in the galaxy are given by $\psi = \tau_{\rm eff}(\xi) + \phi_P(\xi)$, where

$$\tau_{\rm eff} = \tau(\xi) - \frac{|\boldsymbol{\Omega} \wedge \boldsymbol{\xi}|^2}{2} = \tau(\xi) - \frac{\Omega^2(\xi_1^2 + \xi_2^2)}{2} \tag{15}$$

and $\tilde{\Omega}^2(r_g) = 2$, where the normalization factor is that in (14).

The surfaces of constant effective CTF are cylindrical hyperboloids with the generatrix parallel to $\tilde{\xi}_2$ (and so no force acts in this direction). The CTF is expansive along the $\tilde{\xi}_1$ direction, compressive in the $\tilde{\xi}_3$ direction and neutral along the $\tilde{\xi}_2$ direction, no matter what distance the galaxy is from the cluster centre. If $q = 1$ (constant cluster density) then the surfaces become plane-parallel to the orbital $\tilde{\xi}_1 - \tilde{\xi}_2$ plane, and the CTF is compressive along $\tilde{\xi}_3$ and zero in the other two directions. The zero-velocity surfaces of the sum of the CTF and (3) are no longer characterized by axial symmetry around $\tilde{\xi}_1$, as in the case of a radial galaxy orbit.

In Fig. 3 the sections of the zero-velocity surfaces are shown with respect to the principal planes for the two radii marked with dark diamonds in Fig. 1. The upper panels refer to the orbit inside the cluster core radius, and the lower ones to the orbit outside it. In both cases the surfaces show a more pronounced tendency towards prolateness in the cluster radial direction than in the case of the radial orbit. The transition to an observable deformation is around $4R_c$.

3.4 Adiabaticity

If the time-scale of change of the CTF due to the galaxy motion is long compared to the galaxy dynamical time, then the assumption that the galaxy is in local equilibrium with the CTF is correct. If the reverse is the case, or the two time-scales are comparable, the assumption of equilibrium is a poor one, the shape of the galaxy at any time may be significantly different from that of the zero-velocity surfaces, and N-body simulations are required. In order to obtain quantitative information about this time-scale, we introduce a *radial* and a *tangential* characteristic tidal time:

$$\frac{1}{t_{\rm Ti}} \equiv \left| \frac{\mathrm{d} \ln |\mathscr{T}_{ii}[r_g(t)]|}{\mathrm{d}t} \right| = v_{\rm ff}(r_g) \left| \frac{\mathrm{d} \ln |\mathscr{T}_{ii}(r_g)|}{\mathrm{d}r_g} \right|, \tag{16}$$

where $t_{\rm T1}$ and $t_{\rm T2} = t_{\rm T3}$ are the radial and the two equal tangential tidal times, respectively, and $r_g(t)$ is the galactic radial orbit of free-fall. The expressions for a generic spherical system are

$$\frac{1}{t_{\rm T1}} = v_{\rm ff}(r) \left| \frac{2/r + (\alpha - 2/r)q}{q - 2/3} \right|, \tag{17}$$

where $\alpha(r) = \mathrm{d} \ln \rho_c / \mathrm{d}r$, and

$$\frac{1}{t_{\rm T2}} = \frac{1}{t_{\rm T3}} = v_{\rm ff}(r) \frac{3(1-q)}{r}. \tag{18}$$

© Royal Astronomical Society • Provided by the NASA Astrophysics Data System

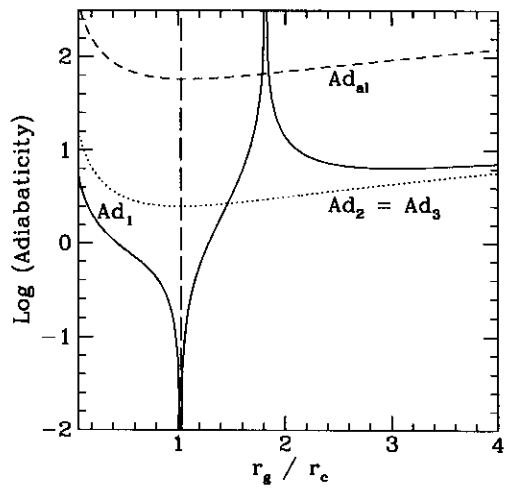

Figure 4. The solid curve (Ad_1) refers to the radial adiabaticity of a galaxy in free-fall from infinity and the dotted curve (Ad_2) is the tangential adiabaticity, i.e. the adiabaticity in the direction perpendicular to the cluster radial direction. The dashed curve (Ad_{al}) is the adiabaticity of a prolate galaxy in a circular orbit around the cluster centre.

We use

$$v_{ff}(r_g) = \sqrt{2|\phi_c(r_g)|} = \sqrt{8\pi G\rho_{co}r_c^2 \mathrm{arsinh}(\tilde{r}_g)/\tilde{r}_g},$$

i.e. for simplicity a fall from infinity. In the above, ϕ_c is the cluster potential. With this choice we are overestimating the rapidity with which the CTF is changing in the galaxy reference system. We define the *adiabaticity* of the galaxy along $\tilde{\xi}_i$ to be the dimensionless number $Ad_i \equiv t_{Ti}/t_{dyn}$. Then the condition $Ad_i \gg 1$ means that the galaxy can 'adjust' its shape along $\tilde{\xi}_i$ to the local CTF. Moreover, one can have the galaxy adiabatic in one direction and non-adiabatic in another. In Fig. 4 the solid line refers to the radial adiabaticity and the dotted line to the tangential one. The radial adiabaticity line divides the cluster into three regions: a very central adiabatic region ($\tilde{r}_g \leq 0.4$), a non-adiabatic intermediate zone ($0.3 \leq \tilde{r}_g \leq 1.3$), and finally the external adiabatic zone. From the divergence of Ad_1 near the cluster core, due to the topological change of the isopotential surfaces at that point, every galaxy in a radial orbit with an apocentre greater than r_c experiences a non-adiabatic radial transition. On the other hand, galaxies with the same parameters as our model are in local equilibrium with the tangential CTF at any distance from the centre. The divergence of the adiabaticity for $\tilde{r}_g \simeq 1.8$ is due to the fact that at this point the radial component of the CTF presents a maximum, i.e. its derivative is zero. From the definition of adiabaticity the divergence follows. From a physical point of view, a galaxy crossing this point experiences no variation of the radial tidal field. Therefore the excursion of Ad_1 near $r_g = 1.8r_c$ is of mathematical interest only and has no important consequences for the physics of the situation.

As far as the alignment problem is concerned, a rough estimate of the characteristic time of response of the prolate model in a circular orbit to the torque induced by the CTF can be easily obtained. Assuming the galaxy to be a rigid body with the major axis in the plane perpendicular to the velocity of its centre of mass, and not considering the non-inertial coupling effect with the other degrees of freedom, one obtains

$$I_{22}\ddot{\theta} = \sin\theta\cos\theta\,(\mathscr{T}_{33} - \mathscr{T}_{11})(I_{33} - I_{11}), \tag{19}$$

where the I_{ii} are the galaxy principal moments of inertia, and θ is the angle between the major axis and the radial cluster direction.

The two points of equilibrium, corresponding to the major axis aligned with ($\theta = 0$) and perpendicular to ($\theta = \pi/2$) the radial cluster direction, are respectively stable and unstable, as in our model $I_{33} - I_{11} > 0$ and, from (12), $\mathscr{T}_{33} - \mathscr{T}_{11} < 0$. Equation (19) is easily solved using elliptic functions, but for our needs it is sufficient to obtain the period by its linearization:

$$\frac{1}{t_{al}} = \frac{\sqrt{4\pi G\bar{\rho}_c}}{2\pi}\sqrt{\frac{(1-q)|1-\lambda|}{1+\lambda}}, \tag{20}$$

where q is given in (13). The behaviour of the adiabaticity associated with these oscillations, $Ad_{al} = t_{al}/t_{dyn}$, is shown for our assumed galaxy and cluster parameters in Fig. 4 (dashed line). One can see that the galaxy is completely adiabatic to the alignment, i.e. a 'mean' star inside it completes many orbits in one oscillation period. Of course the approximation of the galaxy by a rigid body to study the alignment is not correct. What the analysis tells us is that the alignment should be reached in very few, if not only one, oscillation periods.

4 NUMERICAL METHOD

We have shown from the previous qualitative analysis that the problem of a galaxy in the cluster tidal field is intrinsically time-dependent over most of the volume of the cluster, and so it is necessary to use direct N-body simulations to obtain further insight in the subject.

For the problem of galactic deformation the initial conditions are fixed by generating an N-body system from the distribution function,

$$f = \frac{24\sqrt{2}}{7\pi^3}\frac{r_p^2(-E)^{7/2}}{G^5M_g^4}, \tag{21}$$

where E is the total energy for unit mass of an individual star and f is zero for positive energy values. This corresponds to the density profile (2) with global isotropic velocity dispersion (e.g. Aarseth, Hénon & Wielen 1974). In order to reduce the possible initial noise due to the realization of the density distribution with a finite number of particles, the model is evolved for a few dynamical times, maintaining as fixed its initial position in the cluster.

Generation of the initial conditions for the simulations to check the alignment effect is somewhat trickier. In this case no analytical inversion exists to convert the density distribution (6) to a phase-space density distribution. We simply assume the distribution function to be

$$f = \frac{\rho(\varpi, z)}{(2\pi)^{3/2}\sigma_\varpi^2\sigma_z}\exp\left[-\frac{1}{2}\left(\frac{v_\varpi^2}{\sigma_\varpi^2} + \frac{v_z^2}{\sigma_z^2}\right)\right], \tag{22}$$

where σ_z and σ_ϖ are the velocity dispersions in the direction of the major axis and in the plane perpendicular to it, respectively. The spatial dependence of the velocity dispersions is evaluated by numerically solving the Jeans equations in cylindrical coordinates under assumptions of axisymmetry. The

© Royal Astronomical Society • Provided by the NASA Astrophysics Data System

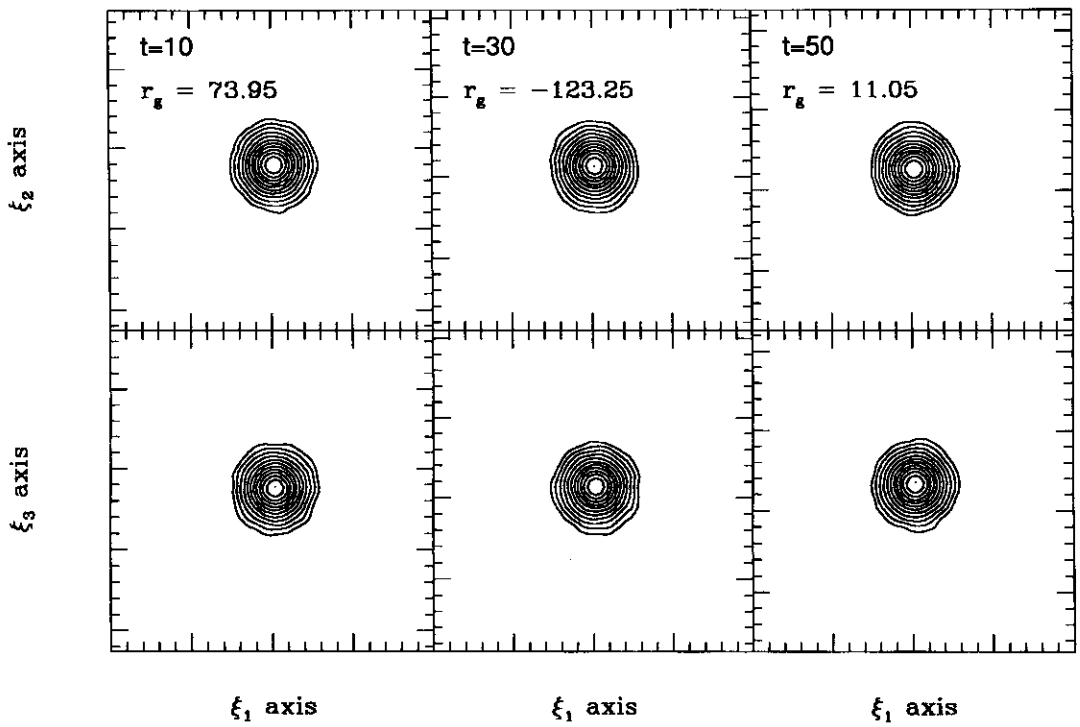

Figure 5. In the lower panels the isodensity contours of the projected galaxy density in the $\xi_1 - \xi_3$ plane are shown. The galaxy is in a radial orbit that is always inside the cluster core radius, and passes through the centre twice during the simulation. The time is expressed in simulation units, and the space between two ticks corresponds to 4.25 kpc. The distance r_g from the centre of the cluster is expressed in kpc. In the upper panels the projection of the density in the $\xi_1 - \xi_2$ plane is shown.

Table 1. Maximum (bottom row) and minimum (top row) isophotal ellipticities of the spherical model between 0.5 and $3.5R_e$. The projection plane is indicated by the subscripts and all values are given for the last simulation time reported in the figures.

Ellipticity	RI_{12}	RI_{13}	RO_{12}	RO_{13}	CI_{12}	CI_{13}	CO_{12}	CO_{13}
ϵ_m	0.00	0.00	0.02	0.00	0.00	0.00	0.01	0.00
ϵ_M	0.09	0.09	0.09	0.07	0.04	0.07	0.07	0.08

required potential ϕ is calculated analytically in the usual way used for the ellipsoidal bodies (see e.g. BT87, pp. 49-62) (the distribution function obtained in this way is clearly not self-consistent, being correct only to the second moment, but the model results in a sufficiently stable initial equilibrium). This galaxy is let loose in the cluster to move in a circular orbit. We choose the initial conditions for the galaxy to be such that its major axis is oriented at an angle of 45° to the line joining the centre of mass of the galaxy and the centre of the cluster, and in the plane perpendicular to the velocity of the centre of mass.

For all the simulations we use the Barnes & Hut (1987) code with minor modifications and the addition of a subroutine that calculates the force due to the cluster. The number of particles is fixed at $N = 32\,768$, and the equivalent simulation time is chosen to be shorter than the two-body relaxation time of the models. We use not the analytical approximation to the tidal field, but the true field of the cluster. In this way we also take the non-linear part of the external field into account. All the times reported in the figures showing the results of the numerical simulations are expressed in *simulation time units* (t_{num}), with $t_{num} \simeq 0.5t_{dyn}$ and $t_{num} \simeq 0.33t_{dyn}$ for the spherical and the prolate models, respectively.

5 RESULTS

We have converted the end-products of the simulations into a density distribution smoothed with a Gaussian described by a smoothing length equal to about 1.5 times the force softening parameters of the code. In the simulation units the force softening is 0.2 while the boxes in Figs 5–9 are 10, which corresponds to 85 kpc. The space between two ticks is 4.25 kpc. If the mass-to-light ratio is constant then the shape of the projected mass distribution will be the same as that of the projected light distribution. After projection we study the model surface density in the same way that the observers study the surface brightness distribution, using IRAF, one of the most-used image processing packages. The projected density distribution of models is fitted using 11 isophotes, and the difference between two consecutive isophotes is equal to 0.5 mag. The intensity difference from the centre to the outer isophote in the figures is 5.5

© Royal Astronomical Society • Provided by the NASA Astrophysics Data System

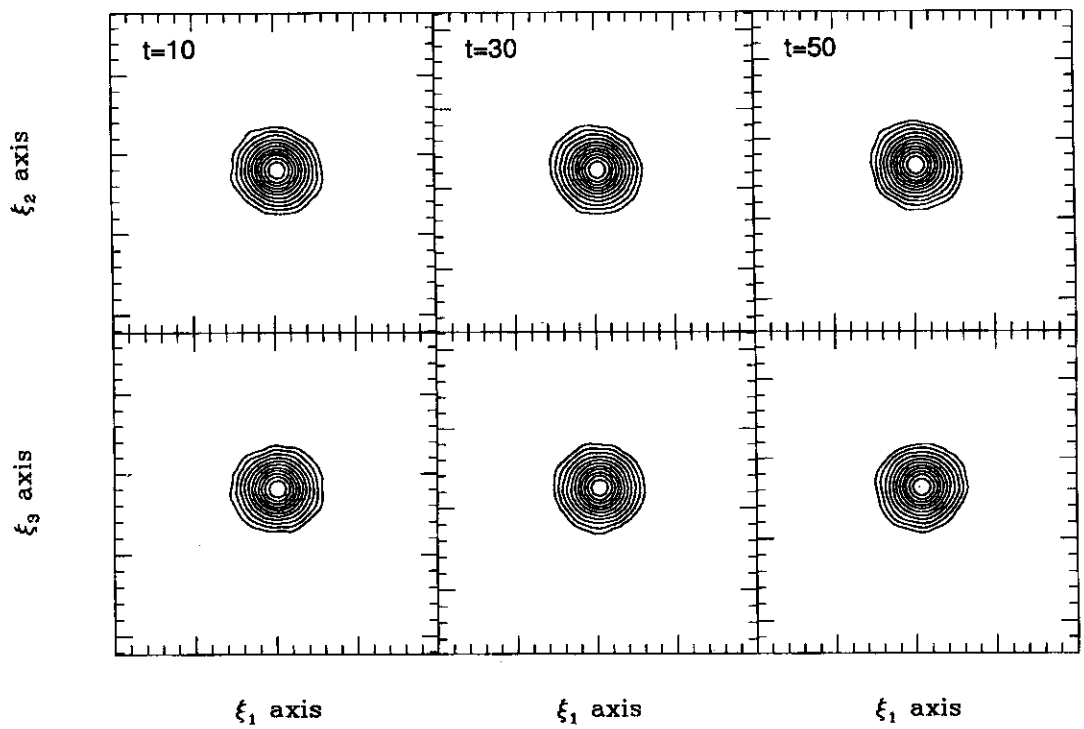

Figure 6. In the lower panels the isodensity contours of the projected galaxy density in the $\xi_1 - \xi_3$ plane are shown. The galaxy is in a circular orbit at $\tilde{r}_g = 0.75$. The time is expressed in simulation units, and the space between two ticks corresponds to 4.25 kpc. In the upper panels the projection of the density in the $\xi_1 - \xi_2$ plane is shown.

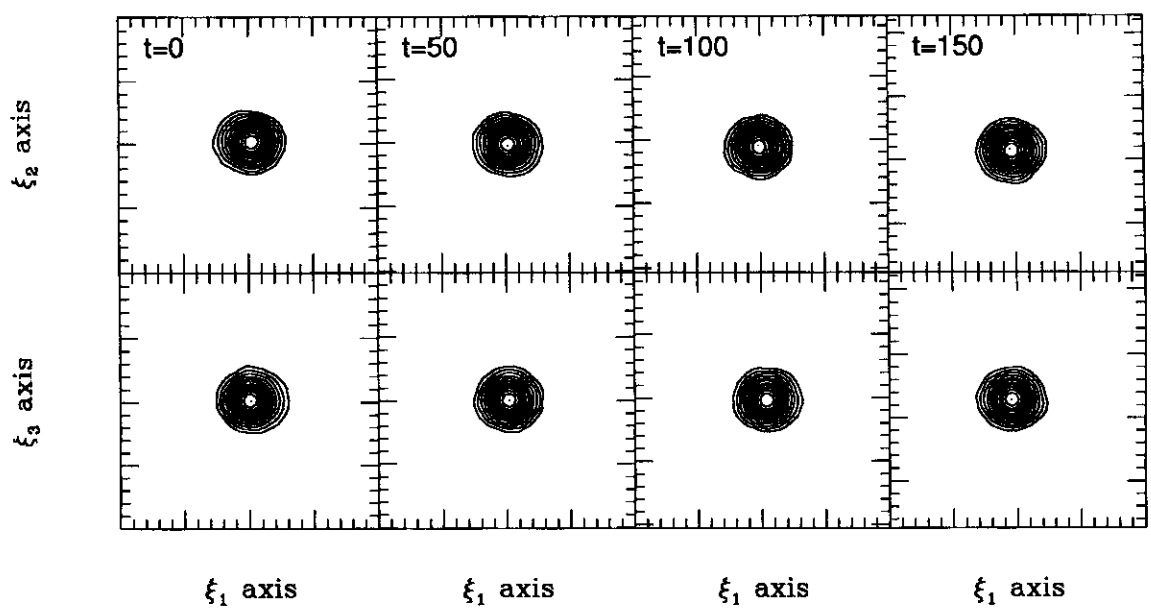

Figure 7. In the lower panels are shown the isodensity contours of the projected galaxy density in the $\xi_1 - \xi_3$ plane. The galaxy is in a circular orbit at $\tilde{r}_g = 1.5$. The time is expressed in simulation units, and the space between two ticks corresponds to 4.25 kpc. In the upper panels the projection of the density in the $\xi_1 - \xi_2$ plane is shown.

mag, and using (5) and (8) this results in approximately a radial range of $3.5R_e$ for the spherical model and $3.85l_e$ for the prolate model, in the projection plane containing the major axis.

5.1 Shape modifications

We ran four simulations of an initially spherical galaxy in a cluster. The model was placed on two radial and two circular

© Royal Astronomical Society • Provided by the NASA Astrophysics Data System

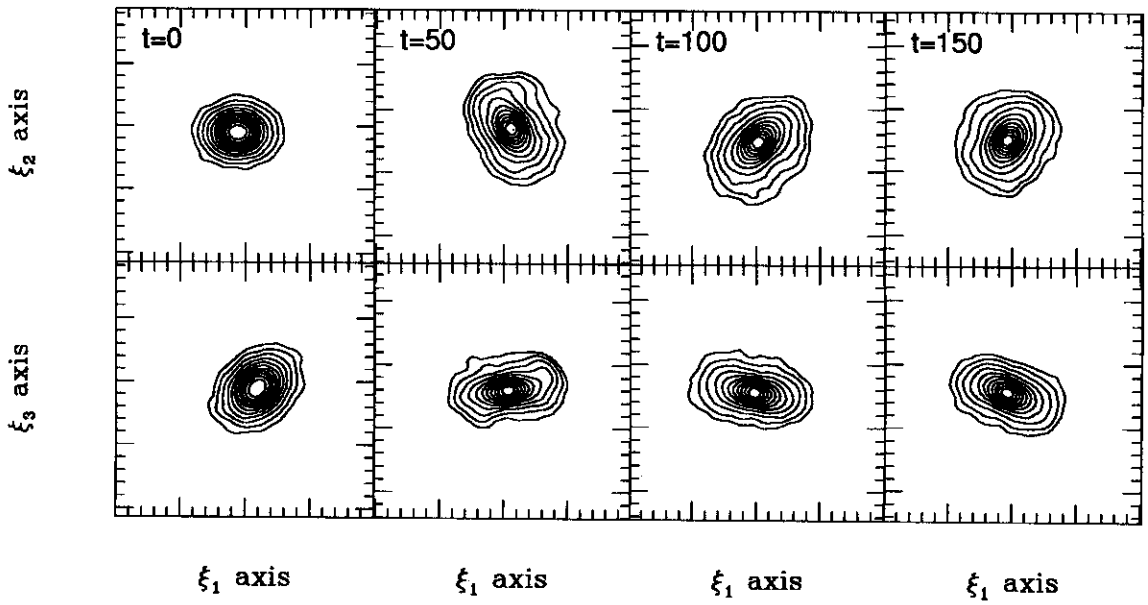

Figure 8. The isodensity contours of the projected galaxy density in the $\xi_1 - \xi_3$ plane and in the $\xi_1 - \xi_2$ plane are shown respectively in the lower and upper panels. The galaxy is in a circular orbit at $\tilde{r}_g = 0.5$. Time is expressed in simulation units, and the space between two ticks corresponds to 4.25 kpc.

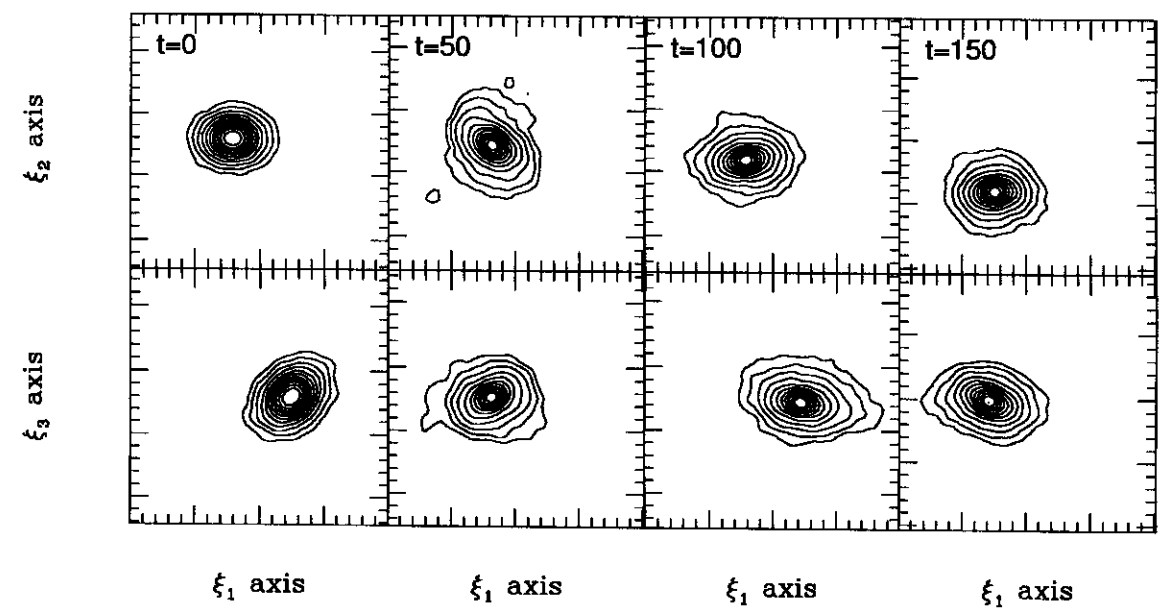

Figure 9. The isodensity contours of the projected galaxy density in the $\xi_1 - \xi_3$ (bottom panels) and $\xi_1 - \xi_2$ (top panels) planes are shown. The galaxy is in a circular orbit at $\tilde{r}_g = 1.5$. Time is expressed in simulation units, and the space between two ticks corresponds to 4.25 kpc.

orbits. One of the radial orbits had its apocentre inside the cluster core radius ($0.75r_c$) while the other had it outside ($1.5r_c$). Similarly, one of the circular orbits lay inside the cluster core radius ($0.75r_c$, at which the circular orbital time in the cluster is $T_{orb} \simeq 7 \times 10^8$ yr) while the other lay outside ($1.5r_c$, with $T_{orb} \simeq 10^9$ yr).

We start by showing the case of the galaxy in the radial orbit that is always inside r_c. In the lower panels of Fig. 5, the isodensity contours of the projected density in the $\xi_1 - \xi_3$ plane at different simulation times are shown. The galaxy orbit is along the ξ_1 axis, and at the beginning of the numerical simulation the galaxy was kept stationary at a distance of $0.75r_c$ for $20t_{num}$ as discussed in Section 4, and then released at zero velocity. In the upper panels of Fig. 5 the same galaxy at the same time is shown, but projected on the $\xi_1 - \xi_2$ plane. It is evident that the galaxy ellipticity is not affected by the CTF. The results of the simulation of a galaxy in a radial orbit with apocentre at a distance of 1.5 times the cluster core radius are essentially equally negative. This is clear from the final ellipticities shown in Table 1. Fig. 4 shows that both

© Royal Astronomical Society • Provided by the NASA Astrophysics Data System

the models in radial orbits cross a region of high radial non-adiabaticity, so we cannot expect a significant effect on the shape of the galaxy. Let us then turn to the investigation of galaxies in circular orbits, as possibly a constant CTF can have a stronger effect in deforming the galaxy.

Fig. 6 shows the evolution of the spherical galaxy in a circular orbit at $\tilde{r}_g = 0.75$. As in the previous cases the galaxy is initially relaxed for the same amount of time, and then released in circular orbit with the initial velocity corresponding to the position of r_g. The galaxy is allowed to complete ~ 0.8 orbits around the cluster centre. It is evident that, in this case as well, the deformation induced on the galaxy is negligible.

In Fig. 7 the projected isodensity contours of the model in a circular orbit at $\tilde{r}_g = 1.5$ are shown. The lower four panels are the projected density distributions in the $\xi_1 - \xi_3$ plane, and the upper four panels the projections in the $\xi_1 - \xi_2$ plane. The model is initially relaxed and released as in the previous simulation. This is the most favourable case for the tidal forces to produce an effect on the shape of the galaxy, so the simulation was continued for $75t_{dyn}$, i.e. ~ 1.7 orbits around the cluster centre. But in this case as well there is no indication of any modification of the galaxy shape.

So, even in the case of circular orbits, i.e. a situation that is intrinsically stationary, the effect of the CTF on the model shape is not observable. In Table 1 the maximum and minimum ellipticities, defined as usual as $\epsilon = 1 - b/a$, are shown for the projected models in two different planes. The particular model is indicated by the labels that refer to the orbit (i.e. CI_{12}=model in circular orbit inside the cluster core radius, projected in the $\tilde{\xi}_1 - \tilde{\xi}_2$ plane). We conclude that we do not expect any systematic difference in shape between cluster Es and field Es induced by the CTF.

5.2 Isophotal alignment

We describe now the evolution of an initially prolate galaxy with its major axis placed in the $\xi_1 - \xi_3$ plane and inclined at 45° to the orbital $\xi_1 - \xi_2$ plane. The orbit of the galaxy centre of mass is circular, with $\tilde{r}_g = 0.5$ ($T_{orb} \simeq 6.3 \times 10^8$ yr), i.e. inside the cluster core. In Fig. 8 the galaxy's density has been projected on to the $\xi_1 - \xi_3$ plane (lower panels).

The galaxy is allowed to complete 2.6 orbits around the cluster centre, but alignment in the radial direction is not reached; only an increase in the ellipticity is evident. In the upper panels of Fig. 8 we plot the projected density of the same simulation in the (orbital) $\xi_1 - \xi_2$ plane. The galaxy remains rounder in this plane due to the assumed initial galaxy configuration. It is clear from this figure that, while there is hardly any isophotal twisting, there is a substantial increase of ellipticity (which was constant with radius at the beginning of the simulation) with time in the outer isophotes, while the inner isophotes stay at about the initial ellipticity. This appears to be true for density projections in and perpendicular to the plane of the orbit.

We move now to the simulation of an identical galaxy with the same initial conditions, the only difference with respect to the previous one being the radius of the circular orbit, now $\tilde{r}_g = 1.5$. Fig. 9 shows the projections of the galaxy density in the $\xi_1 - \xi_3$ and $\xi_1 - \xi_2$ planes. We do observe isophotal alignment in this case, more than for the model in the inner orbit, but not very much isophotal twisting is seen. In this case as well there is evidence for the increase of ellipticity in the outer isophotes, although not quite as dramatic as the case when the galaxy is in a circular orbit inside the cluster core radius. Obviously the first conclusion we can draw from this is that there will be a segregation in the alignment property of elliptical galaxies in clusters. Beyond this, however, is the observation that there is a marked increase of ellipticity with time and this increase is more in the outer isophotes than in the inner isophotes. This is in contrast to the situation for galaxies that were initially spherical, where the CTF appeared to have no effect.

6 CONCLUSIONS

In this paper we report the results of N-body simulations of spherical and prolate Es in a spherical rich cluster. We studied the problem of how the mean tidal field of the cluster affects the Es inside it: we searched for possible galaxy shape deformations and global alignment of prolate galaxies with the cluster radial direction. A preliminary analytical study showed that (i) the topological change in the CTF near r_c causes galaxies on radial orbits through this region to see non-adiabatic potential changes, and (ii) the alignment times for prolate galaxies are much longer than their dynamical time-scales. The galaxy models are placed in circular and radial orbits. The main results are (confirming the analysis in Section 3) that the shape modifications produced by the CTF on the spherical models are not detectable up to many effective radii, but a substantial major axis alignment with the cluster radial direction is reached in a few galactic dynamical times for the prolate galaxies on circular orbits outside the cluster core radius. This alignment is due to the torque induced by the tidal field on the galaxy inertia tensor, and to the conversion into disordered stellar motion of the ordered rotational energy acquired by the galaxy. We suggest a possible population segregation as a function of distance of the galaxy from the cluster centre. The galaxies that are outside the cluster core radius will have a greater tendency to have their major axes aligned in a few internal dynamical times in the direction to the cluster centre than will the galaxies inside the cluster core radius. This effect allows us to reconcile a global galaxy alignment with a bottom-up galaxy formation scenario. We observe in our simulations an increase of the ellipticity of the external isophotes. This is due to the fact that the tidal force increases linearly with the distance from the centre of the galaxy, while the ratio of the self-gravity of the galaxy and the CTF decreases in the outer galaxy regions as the third power of the distance from the galactic centre. We also found no systematic isophotal twisting of the galaxies, and this is consistent with the observational results of Fasano & Bonoli (1989), which exclude the possibility of the CTF being the major contributor to the isophotal twisting in Es.

ACKNOWLEDGMENTS

We are grateful to Jerry Ostriker and David Spergel for useful discussions, to Ralf Bender, George Djorgovsky and Massimo Stiavelli for comments on the observational section, and to Joshua Barnes for kindly providing the code used for the numerical simulations. One of us (LC) acknowledges the warm hospitality of the Princeton University Observatory, where he

© Royal Astronomical Society • Provided by the NASA Astrophysics Data System

was supported by NSF Grant AST 9108103. SND acknowledges the support of NSF Grants AST88-58145 and AST91-17388. This work was partially supported by EEC contract No. CHRX-CT92-0033 and by the Italian Ministry of Research (MURST).

REFERENCES

Aarseth S.J., Hénon M., Wielen R., 1974, A&A, 37, 183
Adams M.T., Strom K.M., Strom S.E., 1980, ApJ, 238, 445
Arnold V.I., 1978, Mathematical methods of classical mechanics. Springer-Verlag, New York
Barnes J., Hut P., 1987, Nat, 324, 446
Binney J., Tremaine S., 1987, Galactic dynamics. Princeton Univ. Press, Princeton (BT87)
Djorgovski S.G., 1987, in Faber S., ed., Proc. of the Santa Cruz Workshop, Nearly Normal Galaxies. Springer-Verlag, Berlin, p.227
Fasano G., Bonoli C., 1989, A&AS, 79, 291
Fong R., Stevenson P.R.F., Shanks T., 1990, MNRAS, 242, 146
Hawley D.L., Peebles P.J.E., 1975, AJ, 80, 477
King I.R., 1972, ApJ, 174, L123
Lambas D.G., Maddox S.J., Loveday J., 1992, MNRAS, 258, 404
MacGillivray H.T., Dodd R.J., 1979a, MNRAS, 186, 69
MacGillivray H.T., Dodd R.J., 1979b, MNRAS, 186, 743
Porter A.C., Schneider D.P., Hoessel J.G., 1991, AJ, 101, 1561
Rhee G., Roos N., 1990, MNRAS, 243, 629
Thompson L.A., 1976, ApJ, 209, 22
Trevese D., Cirimele G., Flin P., 1992, AJ, 104, 935
Valluri M., 1993, ApJ, 408, 57

This paper has been produced using the Blackwell Scientific Publications TEX macros.

© Royal Astronomical Society • Provided by the NASA Astrophysics Data System